Estuarine, Coastal and Shelf Science 183 (2016) 249–259

Contents lists available at ScienceDirect

Estuarine, Coastal and Shelf Science

journal homepage: www.elsevier.com/locate/ecss

Water age in the Columbia River estuary

Tuomas Kärnä*, António M. Baptista

NSF Science and Technology Center for Coastal Margin Observation & Prediction, Oregon Health & Science University, Portland, OR, USA

ARTICLE INFO

Article history:
Received 4 March 2016
Received in revised form
30 August 2016
Accepted 3 September 2016
Available online 6 September 2016

Keywords:
Residence time
Water renewal
Water age
Circulation model
Columbia river estuary

ABSTRACT

The concept of water age is applied to the Columbia River estuary to investigate water renewing time scales. Water age tracers were implemented in a three-dimensional circulation model. The model was run for a nine month period in 2012, covering both high and low flow conditions. In the lower estuary renewing water age ranges from roughly 20 h during high flow season (typically April–June) to 70 h during lowest river discharge (typically September–October). The age of riverine water is strongly dependent on river discharge. Dense oceanic waters, in contrast, are always relatively young in the estuary (roughly 20 h) although their age does vary with tidal range and river discharge. Compared to the main channels, water age tends to be larger in the lateral bays throughout the simulation period; this is especially true under low flow and neap tides conditions when water age can exceed 120 h in the bays. During low flow conditions a strong lateral circulation pattern emerges and leads to higher water age near Grays Bay. The maximal water age in the main channels is associated with mixed water mass (around 6–12 psu) located in front and above the salt wedge. The circulation model results are used to derive simple regression models that can be used to predict renewing water time scales without the need of a circulation model.

1. Introduction

Transport time scales of water in estuaries are important for understanding the fate of pollutants and assessing the likelihood of microbial activity (Wolanski, 2007; Crump et al., 2004; Lucas et al., 2009). The time scale of physical exchange of water is also one of the characteristic parameters of estuaries (Dyer, 1973; Jay et al., 1997; Jay et al., 2000; Valle-Levinson, 2010).

There are many methods for estimating transport time scales. Following Zimmerman (1988) the time scales can be divided into *integrative* and *local* time scales: Integrative time scales (henceforth box-model time scales) apply to the estuary as a whole and yield a scalar time scale for the entire system. They are often derived assuming a perfect and instantaneous mixing within the estuary volume. The simplest box model time scale is the flushing time, i.e. $T_F=V/Q$. T_F is based on the assumption that the entire estuary volume V is flushed by the net outward flux Q. The time scale is usually defined as the e-folding time, i.e. time required to decrease the concentration of initial water to $1/e$ of its initial value. Various box model estimates have been derived to take into account different physical exchange processes (see Andutta et al., 2014, and references therein), for example tidal exchange or estuarine circulation.

In contrast to the box model time scales, local time scales are defined for each point in the estuary. They provide detailed information of the past and/or future of the water masses at the said location. In the Constituent-oriented Age and Residence time Theory (CART, Deleersnijder et al., 2001; Delhez and Deleersnijder, 2002; Delhez et al., 2004; www.climate.be/CART) local residence time is defined as the time that a water parcel at location (x,y,z) and time t is *going to spend* in the estuary. Water age, on the other hand, is defined as the time that a water parcel at location (x,y,z) and time t *has spent* in the estuary.

Local time scales are usually computed with a numerical circulation model, and yield a four dimensional (x,y,z,t) time scale field. Residence time can be solved with an adjoint model that is run backwards in time (Delhez et al., 2004; Zhang et al., 2010; de Brye et al., 2012). The practical difficulty is that the adjoint model is not often available, and integrating the equations backwards in time may not be straightforward. Water age, on the other hand, can be solved with a conventional forward circulation model (Delhez and Deleersnijder, 2002). It does not however provide information of the future fate of the water masses.

Water renewal in estuaries is controlled by the exchange of water at the river and ocean boundaries, driven by the river

* Corresponding author.
E-mail address: karna@ohsu.edu (T. Kärnä).

http://dx.doi.org/10.1016/j.ecss.2016.09.001

discharge and tides. Higher river discharge leads to a lower transport time scale due to stronger residual seaward flow. The influence of the ocean boundary, however, is more complex: Water renewal depends on the strength of estuarine circulation (i.e. density-driven bi-directional flow) and tidal dispersion processes at the ocean boundary (Warner et al., 2010; Shen and Haas, 2004), both of which are influenced by the tides. On the one hand, stronger tides imply stronger mixing, which tends to decrease estuarine circulation, leading into longer transport time scale. On the other hand, stronger tides imply larger tidal excursion and therefore shorter transport time scale. The balance between these competing processes depends on the characteristics of the estuary, and in some cases the forcing conditions.

In this work we use the water age method to study water renewal in the Columbia river estuary. The water age method was implemented in a hindcast circulation model that has previously been shown to capture the main characteristic of the system (Kärnä et al., 2015; Kärnä and Baptista, 2016). The simulation was carried out for a nine month period in 2012 (February 15 to November 15), covering both the river freshet and low flow conditions in the fall. To obtain a system-wide estimate of the water renewal time scale, we computed the *renewing water age* (RWA, de Brye et al., 2012), i.e. the water age that does not differentiate the origin of the waters. In addition, three specific water masses were simulated: riverine, oceanic and plume waters. The oceanic and plume waters, both originating from the estuary mouth, were differentiated by a salinity threshold.

We compare simulated water age values against box model time scales. Simple regression models are used to illustrate how water age depends on the estuary forcing conditions. These models only depend on the river discharge and tidal range, and can therefore be used as predictive tools in cases where running a three-dimensional circulation model is not feasible. We also derive a predictive regression model for the instantaneous RWA, that depends on mean estuary salinity in addition to riverine discharge. These regression models are used to generate long term averages of water age, partially relying on previous multi-annual hindcast simulations for the Columbia River estuary (Kärnä and Baptista, 2016).

2. Columbia River estuary

The Columbia River estuary is a mesotidal estuary characterized by strong river discharge and distinct forcing-dependent flow regimes (Hansen and Rattray, 1966; Jay and Smith, 1990; Geyer and MacCready, 2014). The contemporary annual mean discharge is 5500 m^3s^{-1} and spring freshet typically exceeds 10 000 m^3s^{-1} (Kärnä and Baptista, 2016; Kärnä et al., 2015; Chawla et al., 2008). The maximum daily tidal range varies from less than 1.7 m−3.8 m, and tidal currents can exceed 3 m s^{-1} near the mouth.

Due to strong river discharge the estuary is a rapidly flushing system, typical residence time being of the order of days or less. Despite the short residence time, there are several physical and microbial processes in the estuary that depend on the spatial or seasonal variability residence time. Such processes include the estuary turbidity maxima and biogeochemical processes therein (Prahl et al., 1998;), biogeochemical processes in the lateral bays and marshes (Smith et al., 2015), riverine plankton blooms during spring (Needoba et al., 2012), and estuarine *Mesodinium* spp. blooms in the fall (Peterson et al., 2013). Columbia River estuary is also subject to hypoxia and acidification during low flow season, associated to inflow of dense low-oxygen waters from the ocean (Roegner et al., 2011). To better understand the likelihood and magnitude of such processes, it is important to better characterize the temporal and spatial variability of water masses and their transport time in the system.

The Columbia River estuary is typically classified as a moderately to strongly stratified system during low flow conditions, shifting towards a salt wedge system as flows increase (Hansen and Rattray, 1966; Hughes and Rattray, 1980; Geyer and MacCready, 2014). Recently Kärnä and Baptista (2016) used the Geyer and MacCready (2014) classification scheme in conjunction with long term hindcast simulations to identify four dominant flow regimes that correspond to high/low river discharge and spring/neap tidal conditions. The four regimes, illustrated in Fig. 2, are strongly stratified (low flow, neap tides), partially mixed (low flow, spring tides), salt wedge (high flow, neap tides) and time dependent salt wedge (high flow, spring tides) regimes. This classification scheme is used herein to analyze the magnitude and spatial patterns of water age under different flow conditions.

3. Methods

3.1. Box model estimates

Following Andutta et al. (2014) the flushing time $T_F=V/Q$ can be generalized as:

$$T = \frac{V}{Q_R + Q_D}, \tag{1}$$

where Q_R and Q_D are the volume fluxes at the river and ocean boundary, respectively. Different box model time scale estimates usually differ in their definition of Q_D.

Using the Knudsen salt balance (Knudsen, 1900), results in $Q_D=Q_R S_E/(S_0-S_E)$, where S_0 is the (constant) ocean salinity and S_E, $0<S_E<S_0$ is the mean salinity in the estuary (Andutta et al., 2014). This choice leads into the well-known freshwater fraction time scale,

$$T_{frac} = \frac{S_0 - S_E}{S_0}\frac{V}{Q_R}, \tag{2}$$

which can be interpreted as the renewal time scale of the fresh water mass. While T_{frac} only depends on the river discharge, it does incorporate exchanges at the ocean boundary though the time-dependent mean salinity S_E.

Another choice is to use the salt balance by Fischer et al. (1979) which results in (Andutta et al., 2014)

$$T_{fi} = \frac{S_0 - S_{up}}{S_0 - S_{up} + S_E}\frac{V}{Q_R}, \tag{3}$$

where S_{up} is the up-estuary salinity (salinity at the upstream boundary).

The Land Ocean Interaction Coastal Zone (LOICZ, Swaney et al., 2011) model is obtained by setting $Q_D=Q_R(S_0+S_E)/(S_0-S_E)$ (Andutta et al., 2014):

$$T_{\mathrm{LO}} = \frac{S_0 - S_E}{\frac{3}{2}S_0 - \frac{1}{2}S_E}\frac{V}{Q_R}, \tag{4}$$

Assuming that $S_{up}=0$ (relevant for the Columbia river estuary) we get

$$T_{\mathrm{LO}} < T_{frac} < T_{fi}. \tag{5}$$

We evaluate these time scales from the circulation model. In this work V is taken as the long term mean volume of the estuary as defined by the up- and downstream boundaries used for age tracers (see Fig. 1; $V=2.1\times10^9$ m^3). Value $S_0=34$ psu is used for the ocean

salinity. The mean salinity S_E is computed from the circulation model outputs in the same estuary volume V.

3.2. Water age

Given a well-defined domain of interest, the water age is defined as the time elapsed since water parcel entered the domain (Delhez et al., 1999; Delhez and Deleersnijder, 2002). Here we define the domain of interest by downstream and upstream boundaries located at the mouth of the estuary and upstream Cathlamet Bay, respectively (thick black lines in Fig. 1). Once a water parcel enters the domain either from the river or the continental shelf, it begins to gain "age"; Water age is reset to zero only when the parcel hits either of those boundaries again. Averaging the age of multiple water parcels we can define *mean age*, which becomes a four dimensional field: The mean age at location (x,y,z) and time t stands for the time that water at that location has, on average, spent in the estuary.

Following (Delhez et al., 1999) we compute the water age using an Eulerian approach with a three-dimensional circulation model. A water mass of interest (e.g., riverine water mass) is defined by a passive indicator tracer C that follows the conventional advection-diffusion equation:

$$\frac{\partial C}{\partial t} + \boldsymbol{u}\cdot\nabla C = \nabla\cdot(\boldsymbol{K}\cdot\nabla C), \tag{6}$$

where $\boldsymbol{u}$ is the velocity and $\boldsymbol{K}$ is the diffusivity tensor.

Initially the tracer C is set to zero in the domain. A value 1 is prescribed at the inflow boundary associated with the water mass (e.g., river boundary), while 0 is prescribed on all other boundaries (ocean boundary). As the simulation progresses the concentration C represents the volume fraction that the water mass occupies in the estuary.

The aging of the water mass can be taken into account by the means of an additional tracer, the age concentration α, which has the unit of seconds. The age concentration follows a very similar dynamic equation:

$$\frac{\partial \alpha}{\partial t} + \boldsymbol{u}\cdot\nabla\alpha = \nabla\cdot(\boldsymbol{K}\cdot\nabla\alpha) + C. \tag{7}$$

The only difference to (6) is the additional source term C on the right hand side, which stands for the aging process: α grows by C every second. Age concentration is set to zero initially and on all the boundaries. Finally the mean age is obtained as a ratio of the two tracers,

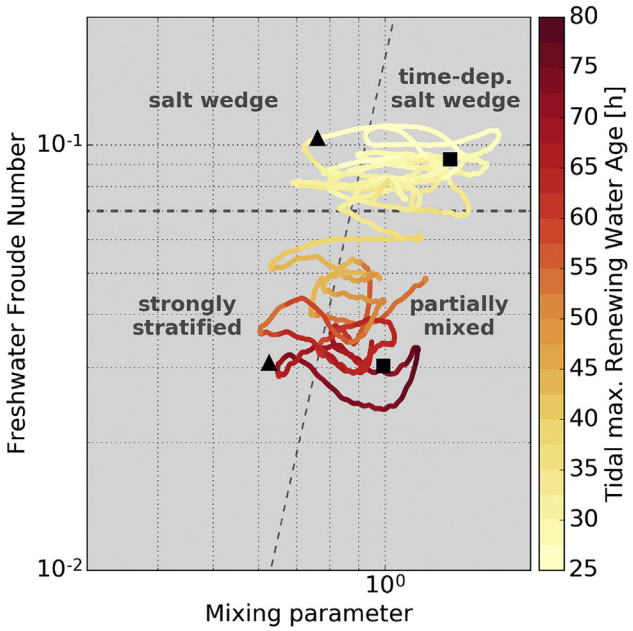

Fig. 2. Renewing water age in the lower estuary channels plotted in the Geyer and MacCready (2014) estuary parameter space for the simulation period. The dashed lines separate the parameter space into the four different flow regimes. The line stands for the state of the estuary during the simulation period, colored by the tidal maximum RWA time series (see Fig. 3 b). The black symbols indicate the four example dates corresponding to each flow regime.

$$a = \frac{\alpha}{C}. \tag{8}$$

The advantage of the water age method is that it is straightforward to implement in any circulation model: typically (6) is already implemented in the model and (7) only requires an additional simple source term. Moreover the Eulerian approach provides a four dimensional age field that covers the entire domain and time span of the simulation.

Here we consider four different water masses. The first water mass is the renewing water, C_{Ren}, defined as water that enters the estuary from either of the boundaries. The associated age, the *renewing water age* (RWA, de Brye et al., 2012), is therefore a proxy for the system's water renewing time scale. Like any other water mass, the concentration of renewing water is initially zero in the estuary. The concentration reaches unity when all the initial waters have been flushed out of the system, which can be used to estimate

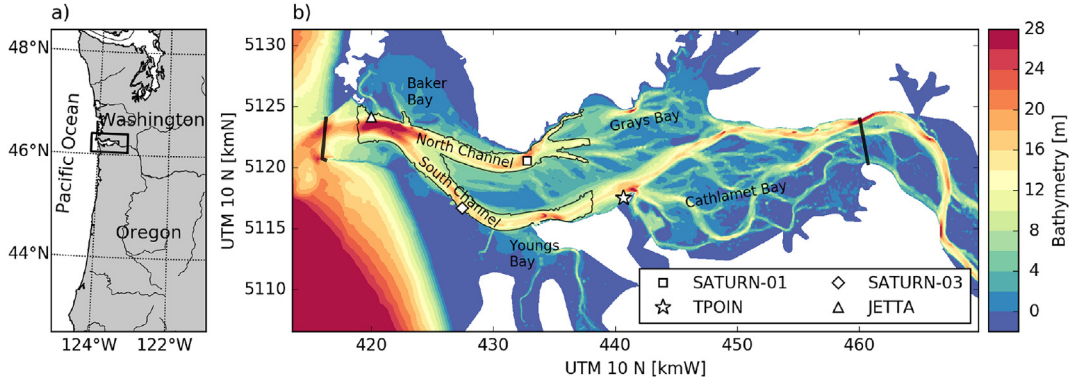

Fig. 1. Geospatial location of the Columbia River estuary (a), and bathymetry of the main estuary (b). The thick lines in (b) indicate the upstream (ocean) and downstream (river) boundaries used in the water age simulations. The thin black line indicates the lower estuary sub-region used in time series analysis.

sufficient model spin-up time.

To investigate the fate of waters from different origins we define three additional water masses: Riverine, oceanic, and plume water mass. The riverine water, C_r, originates from the upstream boundary and is prescribed to zero at the downstream boundary. The oceanic (C_o) and plume (C_p) waters both originate from the downstream boundary and are marked zero at the upstream boundary; They are differentiated by salinity: Waters that enter from the ocean and have salinity greater that 31 psu are labeled as oceanic water; less saline waters are labeled as plume water. This distinction allows tracing the dense oceanic water mass that has important and distinct properties (e.g., low dissolved oxygen). The threshold salinity, 31 psu, was chosen based on the fact that the deep ocean waters are close to 34 psu throughout the year and salinity the main salt wedge in the estuary is close to 32 psu.

It is worth noting that since the riverine, oceanic and plume water masses are mutually exclusive and their sum is always 1 at the boundaries, it is not necessary to simulate the renewing water mass: The concentration and age concentration of the renewing water mass are obtained as the sum of the three individual tracers: $C_{Ren}=C_r+C_o+C_p$ and $\alpha_{Ren}=\alpha_r+\alpha_o+\alpha_p$ (de Brye et al., 2012). The circulation model is therefore embedded with six additional tracers: three indicator and three age concentration tracers.

The simulated water age strongly depends on the location of the up- and downstream boundaries. Moving the river boundary upstream, for example, provides a first-order control on the maximal riverine water age.

3.3. Circulation model

The hydrodynamics of the Columbia River estuary was simulated with the SELFE model (Zhang and Baptista, 2008). The model domain extends from Beaver Army Terminal (85 km upstream of the mouth, not shown) in the riverine end to some 300 km offshore where ocean boundary conditions are imposed from a global ocean model. The model setup is described in detail in Kärnä et al. (2015).

The simulations were carried out between February 15 and November 15, 2012. The indicator tracers were used to determine sufficient model spin-up time; Most of the initial water mass is flushed out of the estuary in roughly 7 days, and after a month the concentration of the initial water mass is below 10^{-3}. The analysis is therefore carried out for the period March 15 to November 15, covering both the high and low flow seasons (Fig. 3a).

Model skill is assessed with the root mean square error,

$$\mathrm{RMSE} = \left(\frac{1}{N} \sum_{i=1}^{N} (y_i - \hat{y}_i)^2 \right)^{\frac{1}{2}}, \tag{9}$$

normalized mean square error,

$$\mathrm{NMSE} = \frac{1}{\sigma_y^2} \frac{1}{N} \sum_{i=1}^{N} (y_i - \hat{y}_i)^2, \tag{10}$$

bias,

$$\mathrm{BIAS} = \overline{\hat{y}} - \overline{y}, \tag{11}$$

and the coefficient of determination

$$R^2 = 1 - \frac{\sum_i (y_i - \hat{y}_i)^2}{\sum_i (y_i - \overline{y})^2} \tag{12}$$

where $\{y_i\}_{i=1}^N$ and $\{\hat{y}_i\}_{i=1}^N$ are the target and predicted time series, respectively, and $\overline{y}$ and σ_y denote the mean and standard deviation of y_i, respectively.

Model skill metrics, evaluated against an extensive observation network (Baptista et al., 2015), are presented in Table 1. Salinity and temperature are well reproduced at JETTA near the mouth where root mean square error is 5 psu and 2 °C, respectively. Performance is poorer in the bottom of the North and South channel (stations SATURN-01 and SATURN-03, respectively). The model performance in general is similar to short-term simulations carried out with the same mesh (Kärnä et al., 2015), as well as a long term hindcast simulation DB33 computed with a mesh that covers the tidal river up to Bonneville Dam (Kärnä and Baptista, 2016). The most significant difference in comparison to the earlier simulations is larger elevation bias, −0.25 m in contrast to typical values within 0.10 m. The difference is related to the boundary condition at Beaver Army terminal (which differs from DB33 setup) and the temporal coverage of the simulation.

3.4. Regression analysis

Time series data sets are analyzed using both linear and exponential regression models. These models are defined by functions

$$y = ax + b, \tag{13}$$

$$y = ax^b, \tag{14}$$

respectively, fitted to (x,y) data sets with the free parameters a,b. The parameters are found with least-squares optimization. Prior to the optimization all the data sets are first interpolated to the same time stamps, using 15 min temporal resolution.

The models are trained using 10-fold cross-validation to avoid over-fitting. The data set is divided into 10 equally sized bins, and the regression model is build using the first nine bins and then tested on the remaining bin. The procedure is repeated 10 times using each bin as test bin exactly once; the reported skill metric is the mean test skill of the 10 regression models.

We also derive a data-driven predictive model for the RWA, inspired by the box model time scale formulas

$$T_{pred} = a \frac{S_0 + bS_e}{S_0 + cS_e} \frac{V}{Q_R}, \tag{15}$$

where (a,b,c) are the free parameters, and S_e stands for mean salinity. This model is trained with the same least-squares optimization.

4. Results

Due to the large amount of data it is not practical to present the raw water age fields. We therefore focus on the temporal and spatial variability of the water age. First, addressing the temporal variability, the age fields are averaged over the main channels in the lower estuary. The resulting time series are then analyzed with respect to the forcing conditions and compared against box model estimates. Spatial variability is addressed in Section 4.2 under each of the four flow regimes.

4.1. Time series analysis

The indicator tracer and water age fields were averaged over a region marked by the thin black line in Fig. 1. This region covers the main channels of the lower estuary where bathymetry exceeds 7.0 m. It was chosen to focus the analysis on the lower estuary where salinity intrusion, estuarine circulation and mixing of water masses are significant.

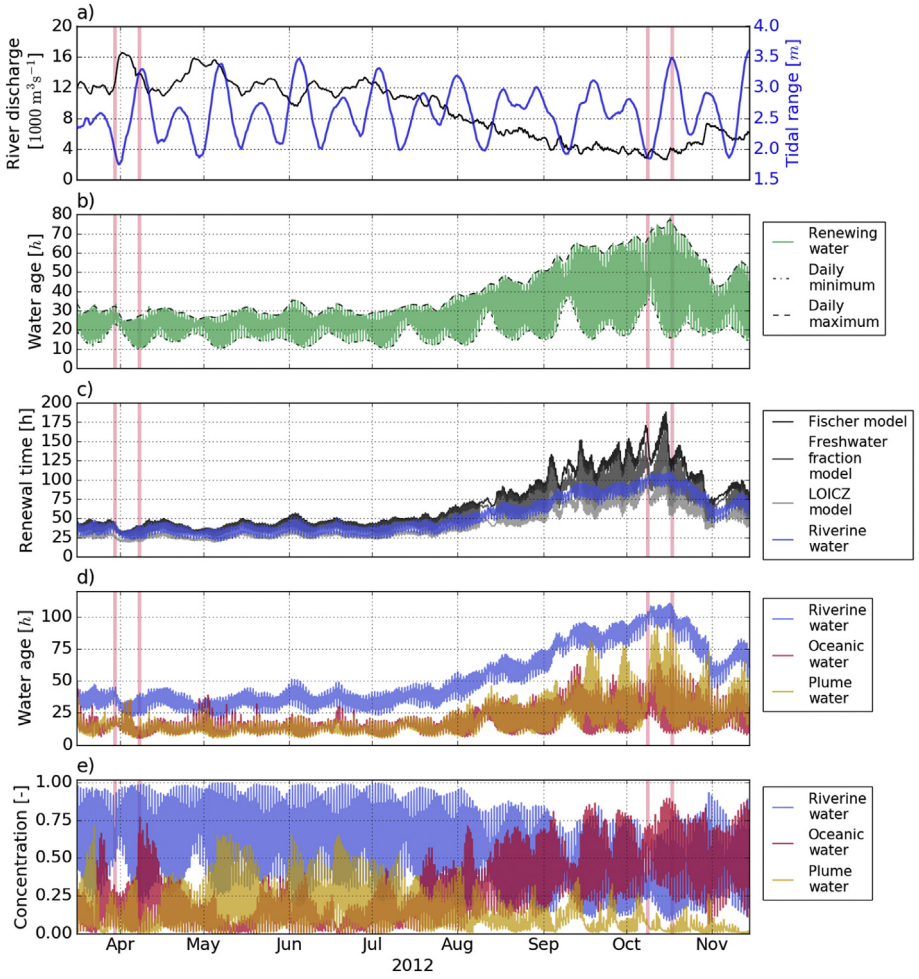

Fig. 3. Time series of the (a) forcing variables, (b) renewing water age, (c) box model estimates compared against age of riverine water, (d) age of the individual water masses and (e) their concentrations. All water age time series are averaged over the lower estuary subregion. The pink vertical bars indicate the four example dates corresponding to each flow regime. (For interpretation of the references to color in this figure legend, the reader is referred to the web version of this article.)

Table 1
Simulation skill metrics for the analysis period March 15 – November 15, 2012. Station locations are shown in Fig. 1.

Variable	Station	RMSE	BIAS	NMSE
Elevation [m]	TPOIN	0.31	−0.25	0.15
Salinity [psu]	JETTA 6.4 m	4.56	1.29	0.19
Salinity [psu]	SATURN-01 19.5 m	12.38	−7.40	1.72
Salinity [psu]	SATURN-03 13.0 m	4.99	−1.48	0.28
Temperature [°C]	JETTA 6.4 m	1.38	−0.10	0.20
Temperature [°C]	SATURN-01 19.5 m	2.81	1.31	1.48
Temperature [°C]	SATURN-03 13.0 m	1.82	0.45	0.49

The time series are presented in Fig. 3, together with the forcing conditions (panel a) as well as box model estimates (panel c). The strong dependency on river discharge is apparent in all the data sets. The RWA ranges from roughly 20 h during the high flow season to maximum 70 h in the low flow season (Fig. 3b). The age of the individual water masses shows similar dependency (Fig. 3d). The riverine water is the oldest and shows less tidal variability.

The average concentration of each water mass is shown in Fig. 3(e). Riverine water dominates during the high flow season. Around August 2012 the fraction of riverine water mass starts to decrease, compensated by significant increase in the oceanic water fraction. The plume water mass becomes very scarce during the low flow season (September–November).

The plume and oceanic water masses appear to complement each other: During high flow conditions the mixed plume waters (salinity less than 31 psu) frequently enter the estuary while intrusion of dense oceanic waters tends to be more scarce. During the low flow season, however, almost all of the waters entering from the ocean are dense. This may have important implications on hypoxia and acidification associated with the dense oceanic water mass, as well as estuary-plume interactions (e.g. associated with algal blooms in the plume, Smith et al., 2015).

4.1.1. Comparison against box model time scales

The three box model water renewal time scales are presented in Fig. 3(c). As expected the Fischer time scale is the highest, followed by the freshwater fraction and the LOICZ model. The age of the riverine water falls between the LOICZ and freshwater fraction estimate. Fitting a linear function to (a_{Ren},T_{frac}) data results in relation,

$$T_{frac} = 1.77\, a_{Ren} + 1.74 \times 10^4 \text{ s}, \tag{16}$$

where a_{Ren} is the mean renewing water age in the lower estuary. The function, illustrated in Fig. 4(a), suggests that T_{frac} is almost twice as large as RWA. Nevertheless the agreement is relatively good: RMSE of the fit is 14 h and the coefficient of determination R^2=0.73.

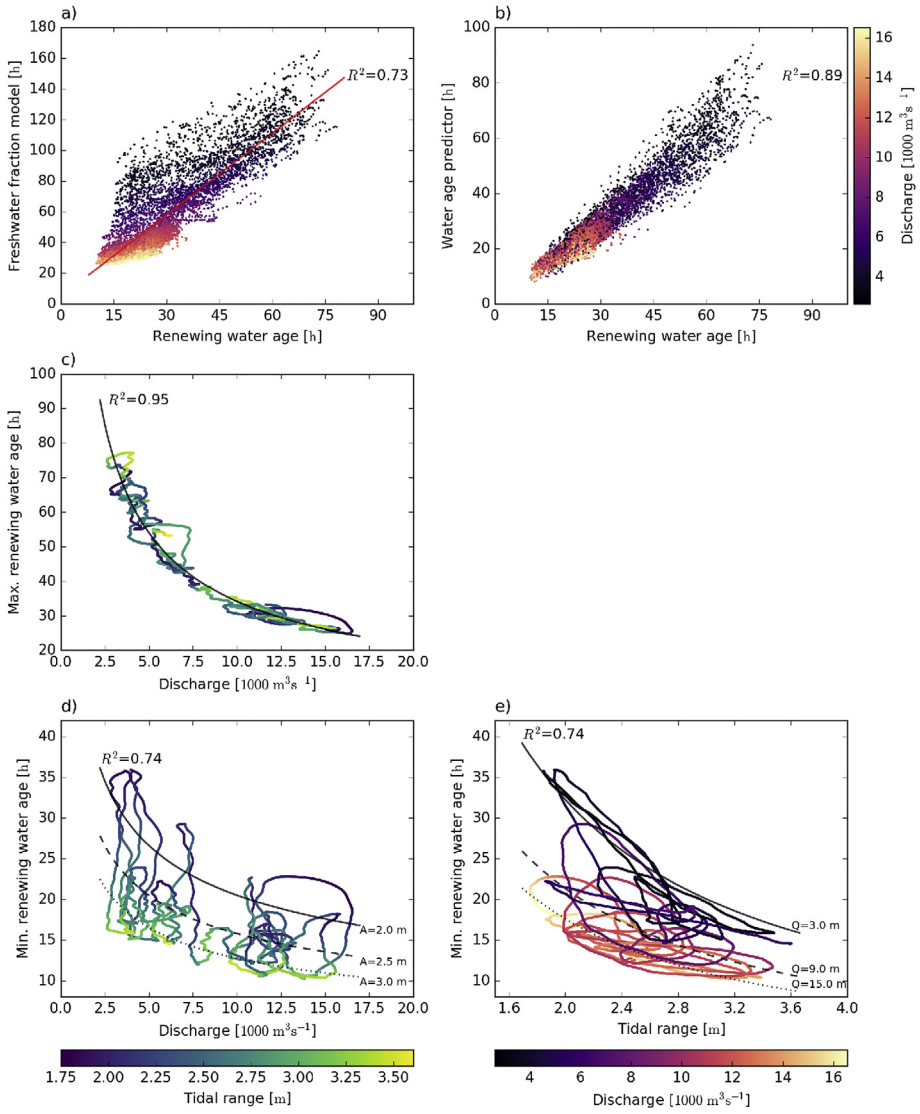

Fig. 4. Scatter plots of (a) freshwater fraction estimate T_{frac}, and (b) water age predictor T_{pred} versus renewing water age a_{Ren}, (c) maximum daily renewing water age $a_{Ren}^{\max}$, and (d, e) minimum daily renewing water age $a_{Ren}^{\min}$ versus river discharge and tidal range. The regression model in (d, e) depends on both the river discharge and tidal range.

In order to obtain a better predictor, we fitted the model (15) to the data sets, resulting in

$$T_{pred} = 0.57 \frac{S_0 - 1.1 S_e}{S_0 - 0.75 S_e} \frac{V}{Q_R}. \tag{17}$$

Here S_e stands for the mean salinity in the same lower estuary subregion. This model, illustrated in Fig. 4(b), resembles the LOICZ formulation and has RMSE 4.3 h and R^2=0.89. Therefore T_{pred} can be used as a predictor in cases where running a water age simulation is not feasible, as long the mean salinity S_e can be estimated.

4.1.2. Dependency on forcing conditions

Fig. 3(b) suggests that the daily maximum RWA is inversely correlated with the river discharge, while the minimum RWA appears to depend on both the discharge and tidal range.

To quantify these dependencies, exponential regression models were fitted to the minimum and maximum envelopes of RWA. Daily minimum and maximum RWA were first computed with a sliding 24.84 h window, and the time series was further low-pass filtered to remove tidal frequencies. The resulting time series are plotted in Fig. 3(b) with dash-dotted and dashed lines, respectively.

In the case of the maximum RWA, the dependency on tidal range was close to zero so river discharge was used as the only explanatory variable, resulting in the model

$$a_{Ren}^{\max} = 5.40 \times 10^7 \text{ m}^3 \; Q_R^{-0.66}. \tag{18}$$

This model, illustrated in Fig. 4(c), has RMSE 3.23 h and R^2=0.95. This dependency indicates that the maximum RWA is associated with the freshwater flushing through the system; maximal RWA is roughly the time it takes for waters to travel from the upstream boundary to the mouth, as the oceanic or plume waters tend to be younger (Fig. 3d).

In the case of the minimum RWA both tidal range and river discharge were used as explanatory variables:

$$a_{Ren}^{\min} = 5.32 \times 10^6 \text{ m}^4 \; Q_R^{-0.38} A_{\text{tr}}^{-1.17}, \tag{19}$$

where A_{tr} denotes the tidal range in meters. In this case RMSE=2.58 h and R^2=0.74. The model is illustrated in Fig. 4(d, e). This model suggests that the tidal range has roughly similar effect

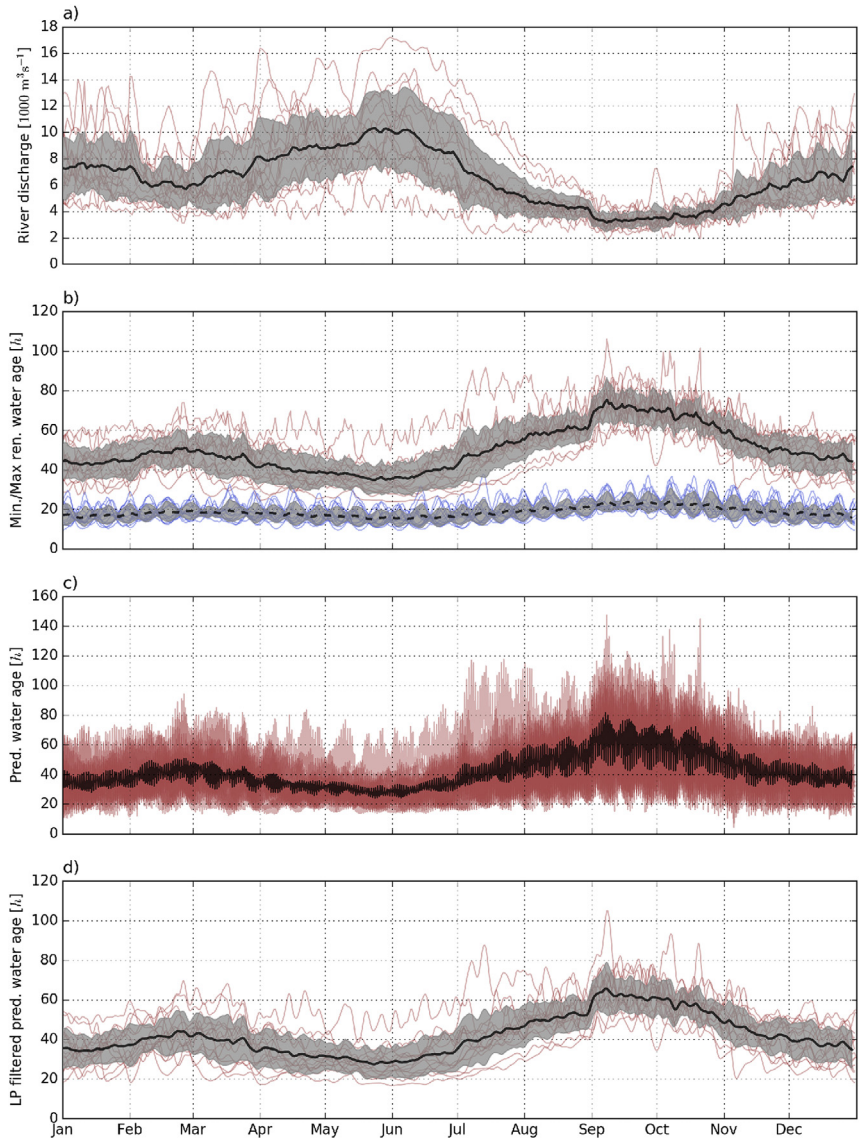

Fig. 5. Predicted long term variability of water age in the Columbia River estuary for years 2000–2014. a) Annual river discharge; b) Maximum and minimum daily water age; c) Predicted water age; d) Low-pass filtered predicted water age. Individual years are marked with blue and red lines. The bold black line indicates the mean; gray shading indicates mean ± standard deviation. Gray shading in (c) is omitted for clarity. (For interpretation of the references to color in this figure legend, the reader is referred to the web version of this article.)

on minimum RWA regardless of the river discharge condition: $a_{Ren}^{\min}$ is roughly 2.2 times higher during neap tides (A_{tr}=1.8 m) compared to spring tides (A_{tr}=3.5 m).

In contrast to the maximum RWA, the minimum RWA is strongly affected by the exchange near the mouth, i.e. the intrusion of younger oceanic and plume water masses. The minimum RWA is lower during spring tides as more young waters enter from the shelf sea due to the larger tidal excursion. This suggests that the Columbia River estuary is an advection dominated system; the effect of mixing and estuarine circulation on RWA is small compared to the effect of tidal excursion.

4.1.3. Long-term variability

The regression models for $a_{Ren}^{\min}$ and $a_{Ren}^{\max}$ only depend on the river discharge and tidal range, both of which can be derived from observations. These models can therefore be used to predict variability of water age in the Columbia River estuary outside the simulated period. Such an extrapolation is possible because the regression models are relatively simple (therefore less prone to overfitting) and because they were trained on a data set that covers the typical river discharge and tidal conditions.

The predicted daily minimum and maximum water age (in the lower channels) is presented in Fig. 5(b) for years 2000–2014. These predictions were obtained with daily Beaver Army river discharge data and tidal range computed form TPOIN water elevations. On average, water age is smallest between April and June due to river freshet; the daily maximum RWA is around 30–40 h. Water age is highest (70 h on average) in September and October when the flow through Bonneville dam is smallest (the sudden jump in the beginning of September is caused by dam regulations). Another maximum (up to 50 h) occurs in February and March just before the freshet, also due to lower river discharge. Daily minimum RWA, associated with the oceanic waters, varies between 10 and 20 h depending on the flow regime and tides.

Fig. 5(c) shows the predicted water age, T_{pred}, for the same years. These results were computed using the same long term river

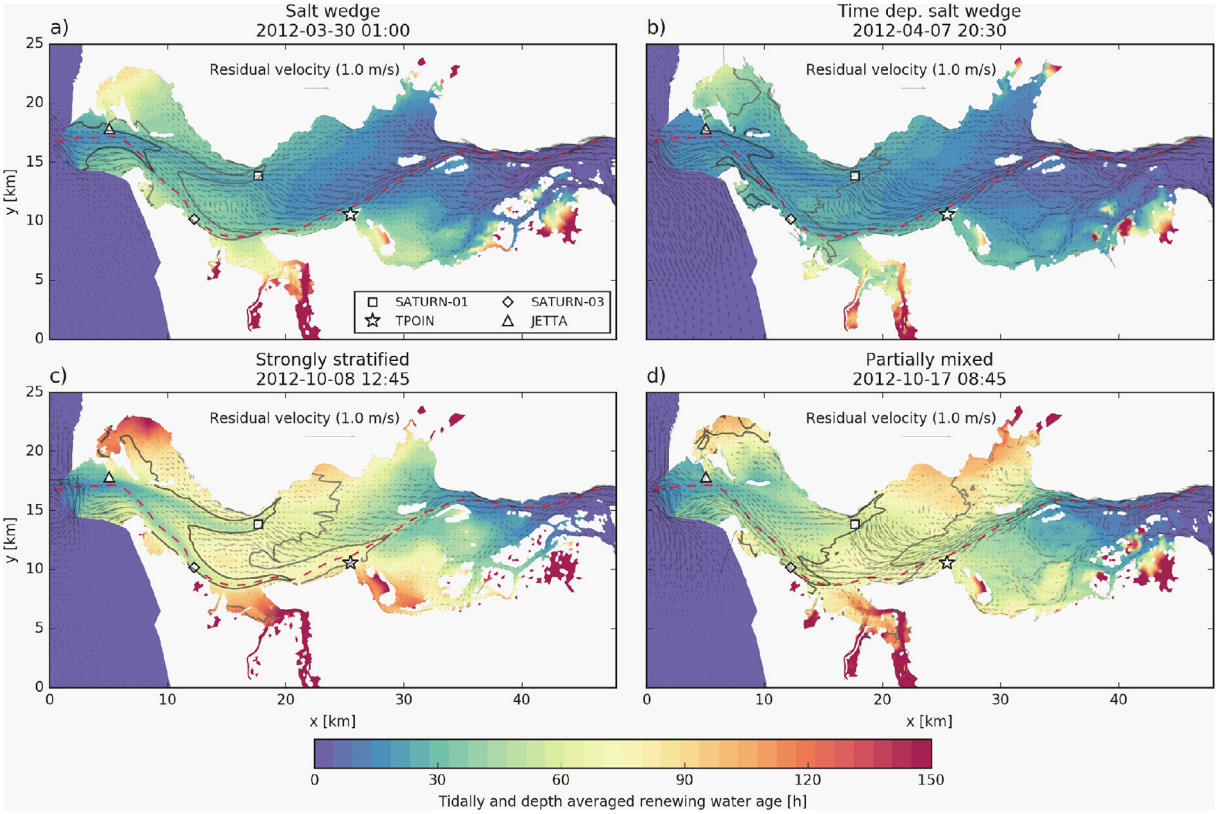

Fig. 6. Tidally and depth averaged renewing water age for the four flow regimes. Gray solid lines indicate isohalines (dark gray, 15 psu; light gray 5 psu). South Channel transect is marked with dashed red line. These maps were created by averaging RWA over the water column and then averaging over a tidal day. In areas affected by wetting-drying the temporal average of wet time steps was computed. (For interpretation of the references to color in this figure legend, the reader is referred to the web version of this article.)

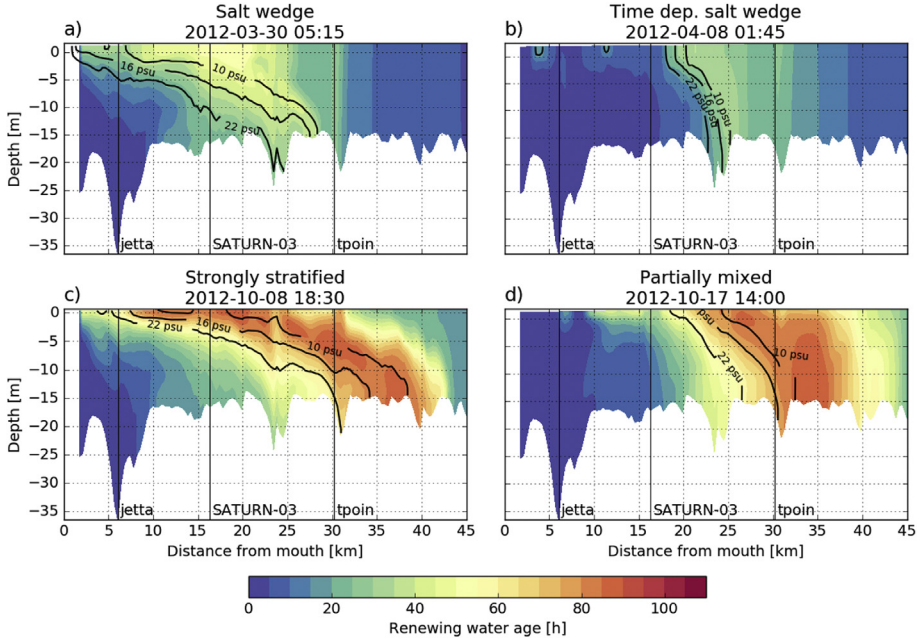

Fig. 7. South Channel transects of renewing water age for the four flow regimes. Location of the transect is show in Fig. 6. Each transect is plotted at higher high water.

discharge and tidal range data as above. In addition the mean estuarine salinity S_e was extracted from a long term hindcast simulation DB33 (Kärnä and Baptista, 2016). Without any filtering T_{pred} varies with tides. The low pass filtered T_{pred} (Fig. 5d) varies between 30 and 60 h for between the high and low flow seasons, and can be taken as a proxy for daily mean water age in the lower estuary.

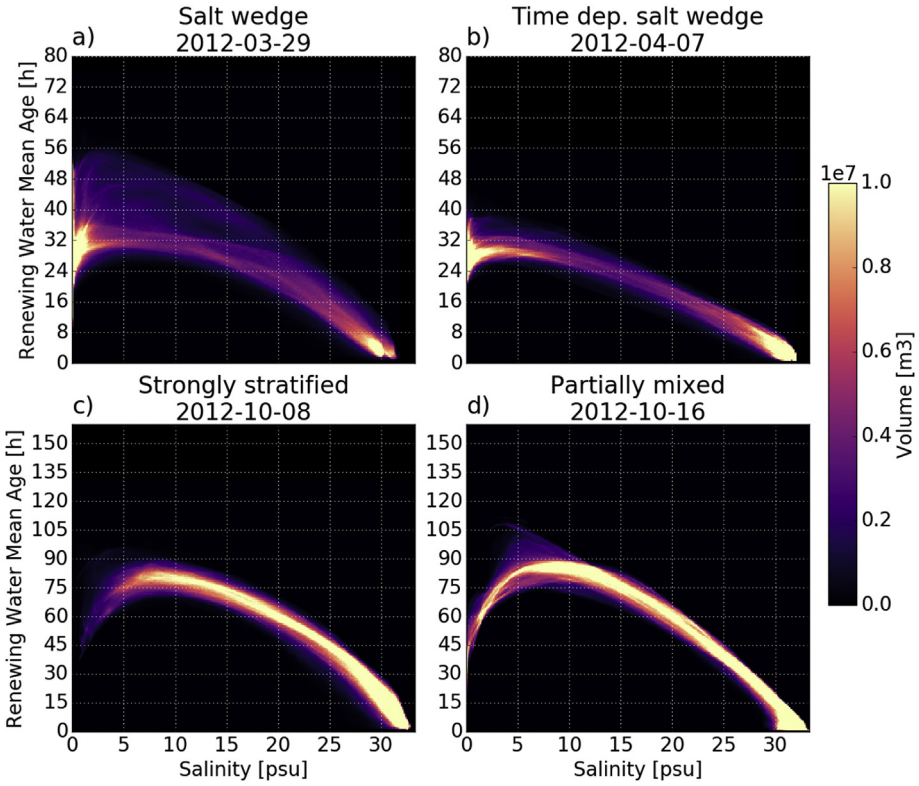

Fig. 8. Volume histogram of waters in the lower estuary channels versus salinity and renewing water age for the four flow regimes. The histograms were computed by taking all the nodal values of the model in the lower estuary sub-region, binning the data against RWA and salinity, and averaging the histogram over a tidal day. During low flow conditions maximal RWA coincides with brackish waters (6–12 psu); the dependency is weaker under high flow conditions when the age of freshwater dominates.

4.2. Spatial variability under different flow regimes

To examine spatial patters of the water age fields, we chose four characteristic tidal days (24.84 h) in each of the flow regimes (Fig. 2). The chosen tidal days begin at: salt wedge, 2012-03-29 12:30 PST; time dependent salt wedge, 2012-04-07 08:00 PST; strongly stratified, 2012-10-08 00:30 PST; partially mixed, 2012-10-16 20:30 PST.

4.2.1. Horizontal variability

Fig. 6 shows maps of depth and tidally averaged RWA fields for the flow regimes. As expected the RWA is maximal in the center of the domain, because the age concentration is small at the vicinity of the boundaries. The maximal RWA tends to coincide with the isohalines of brackish waters.

The influence of river discharge is apparent: high flow regimes (panels a and b) show lower RWA. In the main stem of the estuary RWA can reach approximately 30 h in the salt wedge regime, and 20 h in the time dependent salt wedge regime. During low flows, however, tidally and depth averaged RWA can reach 75 h.

The tides have an effect on the spatial distribution of RWA. In general RWA tends to be lower during spring tides in the main stem of the estuary (panels b and d). As stated earlier this is related to stronger tidal excursion.

In panel (c), however, the RWA is lower in the main channels during neap tides. This effect is related to estuarine circulation: Weaker tides imply weaker mixing and result in stronger estuarine circulation and hence stronger inflow of young oceanic waters in the bottom layer. As tidal excursion is small, however, the oceanic waters do not travel very far upstream and this effect is confined to the deep channels only. Lower RWA is especially clear in the flood-dominant North Channel.

Lateral bays exhibit higher RWA in all the cases. RWA is elevated in the lateral bays especially during neap tides when the bays are flushed less efficiently. This is apparent in Baker Bay, Youngs Bay, and the downstream end of Cathlamet Bay. In these regions RWA can exceed 120 h during strongly stratified regime, while RWA in the main estuary is roughly half of that. The higher water age may be an important factor for various biogeochemical processes in the lateral bays, such as the incubation of *Mesodinium* spp. blooms.

The area downstream of Grays Bay, however, shows increased RWA during partially mixed regime, i.e. low flow and spring tides. This is presumably related to strong tidally-induced lateral circulation around SATURN-01 that is able to retain waters in this area. These results suggest that the lateral circulation pattern emerges under low flow season and tends to increase RWA in the downstream end of Grays Bay. The effect intensifies under spring tides. Under high flow conditions, on the other hand, the strong river discharge dominates and efficiently flushes waters from Grays Bay area.

4.2.2. Vertical variability

Instantaneous RWA transects along the South Channel of the estuary are shown in Fig. 7. RWA varies significantly in the vertical direction as well. In all regimes the maximal RWA is located in front and above the salt wedge, suggesting that the brackish waters are the oldest in the estuary: the relatively dense brackish waters are "arrested" by the salt wedge and cannot therefore be flushed directly to the ocean.

Stratification responds to tidal forcing; it is clearly smaller during spring tides (panels b and d) due to increased mixing. The water column is well mixed especially during high flows (panel b) when

the circulation in the estuary is the most energetic.

The relationship between RWA and salinity is visualized with two-dimensional histograms (Fig. 8). Maximal RWA is associated with brackish salinities (6–12 psu) especially under low flow conditions. Note that fresh water is abundant in the lower estuary channels during high flow conditions (panels a and b), while there is no freshwater under strongly stratified regime (panel c). During high flows the maximal RWA tends to be associated with the fresh water mass.

5. Discussion

We have presented water age simulations for the year 2012, and extrapolated the results to estimate long-term variability for years 2000–2014. Validating water age results against observations is not straightforward; In general simulated age results are as reliable as the underlying circulation model. The skill of the present model has been carefully validated indicating that in general it captures the dynamics of the estuary (Kärnä et al., 2015; Kärnä and Baptista, 2016). The model results may be less reliable in upstream portions of the lateral bays: First, the wetting-drying method used in SELFE may lead to spurious tracer values in the intertidal regions. Second, due to lack of observational data, the lateral bays do not have any freshwater input which may lead to unrealistically high water age. Based on our simulations, however, these effects in the shallow regions do not deteriorate water age results in the main channels because of their small volumetric contribution.

The model results suggest that lateral circulation has a strong impact on the water age in the estuary. First, waters in lateral bays tend to be older compared to the main channels regardless of the flow regime. Consequently RWA in Baker Bay, Youngs Bay, and the downstream end of Cathlamet Bay is high, and may exceed 120 h under low flow and neap tide conditions. Second, under low flow conditions a strong residual lateral circulation pattern emerges around the SATURN-01 station where the ebbing currents shift from the South to the North channel, effectively preventing waters from Grays Bay from flushing out; This local retention feature is stronger during spring tides. The fact that water age is elevated in the lateral bays, may be important for microbiology: These areas may provide a safe haven for biogeochemical activity in otherwise fast-flushing system.

The spatial distribution of RWA suggests that residence time is largest in the brackish water mass. Saline waters tend to be young, their age being controlled by the tides and river discharge that drive salinity intrusion. The age of the fresh water mass, on the other hand, is largely determined by the river discharge. In the lower estuary these end-member waters mix into the brackish water mass, which tends to be older as it is arrested in front of the salt wedge.

The location of maximal water age in the channels coincides with areas of the estuarine turbidity maxima (ETM) in the system (Gelfenbaum, 1983; Jay and Musiak, 1994; Small and Prahl, 2004). Although we did not consider the age of suspended particulate matter in this work, it is possible that microbial organisms in this region benefit from the higher residence time; it is also likely that the age of particulate matter is even more elevated, further increasing the residence time of particle attached microbes.

6. Conclusions

Water age simulation was carried out for the Columbia River estuary for the year 2012. The renewing water age (RWA) is mostly controlled by river discharge; it ranges from roughly 20 h during high flow season (typically May–June) to 70 h during lowest river discharge (typically September–October). Tidal range affects RWA to lesser extent. The estuary is largely occupied with riverine water but intrusion of dense oceanic waters is significant during low river discharge season. Tidal range has a strong impact on the age of the dense oceanic waters, which ranges from 10 h (during high flow and spring tides) to 50 h (low flow and neap tides).

RWA is also strongly dependent on lateral circulation: RWA is higher in lateral bays where circulation is weaker, especially during neap tides, or in areas with strong lateral circulation (Grays Bay during low river discharge). In the main stem of the estuary the highest RWA occurs in the brackish salinity ranges (roughly 6–12 psu).

Simple regression models were derived for predicting the daily minimum and maximum RWA, based on river discharge and tidal range. As the input variables can be derived from observations, these models can serve as predictor tools in cases when running a three-dimensional circulation model is not feasible. These predictors were used to estimate long term variability of water age, shown in Fig. 5.

Acknowledgments

The National Science Foundation partially supported this research through cooperative agreement OCE-0424602. The National Oceanic and Atmospheric Administration (NA11NOS0120036 and AB-133F-12-SE-2046), Bonneville Power Administration (00062251) and Corps of Engineers (W9127N-12-2-007 and G13PX01212) provided partial motivation and additional support. This work used the Extreme Science and Engineering Discovery Environment (XSEDE), which is supported by National Science Foundation grant number ACI-1053575. The authors acknowledge the Texas Advanced Computing Center (TACC) at The University of Texas at Austin for providing HPC resources that have contributed to the research results reported within this paper.

References

Andutta, F.P., Ridd, P.V., Deleersnijder, E., Prandle, D., 2014. Contaminant exchange rates in estuaries – new formulae accounting for advection and dispersion. Prog. Oceanogr. 120, 139–153.

Baptista, A.M., Seaton, C., Wilkin, M.P., Riseman, S.F., Needoba, J.A., Maier, D., Turner, P.J., Kärnä, T., Lopez, J.E., Herfort, L., Megler, V., Mcneil, C., Crump, B.C., Peterson, T.D., Spitz, Y.H., Simon, H.M., 2015. Infrastructure for collaborative science and societal applications in the Columbia River estuary. Front. Earth Sci. 1–24.

de Brye, B., de Brauwere, A., Gourgue, O., Delhez, E.J., Deleersnijder, E., 2012. Water renewal timescales in the scheldt estuary. J. Mar. Syst. 94, 74–86.

Chawla, A., Jay, D., Baptista, A.M., Wilkin, M., Seaton, C., 2008. Seasonal variability and estuary–shelf interactions in circulation dynamics of a river-dominated estuary. Estuar. Coasts 31, 269–288.

Crump, B.C., Hopkinson, C.S., Sogin, M.L., Hobbie, J.E., 2004. Microbial biogeography along an estuarine salinity gradient: combined influences of bacterial growth and residence time. Appl. Environ. Microbiol. 70, 1494–1505.

Deleersnijder, E., Campin, J.-M., Delhez, E.J.M., 2001. The concept of age in marine modelling I. Theory and preliminary model results. J. Mar. Syst. 28, 229–267.

Delhez, E.J.M., Campin, J.-M., Hirst, A.C., Deleersnijder, E., 1999. Toward a general theory of the age in ocean modelling. Ocean. Model. 1, 17–27.

Delhez, E.J.M., Deleersnijder, E., 2002. The concept of age in marine modelling II. Concentration distribution function in the English Channel and the North Sea. J. Mar. Syst. 31, 279–297.

Delhez, E. J. M., Deleersnijder, E., & Rixen, M. (2004). 34th International Liège Colloquium on ocean dynamics. Liège, Belg., May 6-10, 2002. Tracer methods in geophysical fluid dynamics (Preface). Journal of Marine Systems, 48, 1–2.

Dyer, K., 1973. Estuaries: A Physical Introduction. A Wiley-Interscience publication. John Wiley.

Fischer, H., List, J., Koh, C., Imberger, J., Brooks, N., 1979. Mixing in Inland and Coastal Waters. Academic Press.

Gelfenbaum, G., 1983. Suspended-sediment response to semidiurnal and fortnightly tidal variations in a mesotidal estuary: Columbia River, U.S.A. Mar. Geol. 52, 39–57.

Geyer, W.R., MacCready, P., 2014. The estuarine circulation. Annu. Rev. Fluid Mech. 46, 175–197.

Hansen, D.V., Rattray, M., 1966. New dimensions in estuary classification. Limnol. Oceanogr. 11, 319–326.

Hughes, F., Rattray, M., 1980. Salt flux and mixing in the Columbia river estuary.

Estuar. Coast. Mar. Sci. 10, 479–493.
Jay, D., Uncles, R., Largeir, J., Geyer, W., Vallino, J., & Boynton, W. (). A review of recent developments in estuarine scalar flux estimation. Estuaries, 20, 262–280.
Jay, D.A., Geyer, W.R., Montgomery, D.R., 2000. An ecological perspective on estuarine classification. In: Hobbie, J.E. (Ed.), Estuarine Science: A Synthetic Approach to Research and Practice. Island Press, pp. 149–176.
Jay, D.A., Musiak, J.D., 1994. Particle trapping in estuarine tidal flows. J. Geophys. Res. Oceans 99, 20445–20461.
Jay, D.A., Smith, J.D., 1990. Circulation, density distribution and neap-spring transitions in the Columbia River Estuary. Prog. Oceanogr. 25, 81–112.
Kärnä, T., Baptista, A.M., 2016. Evaluation of a long-term hindcast simulation for the Columbia River estuary. Ocean. Model. 99, 1–14.
Kärnä, T., Baptista, A.M., Lopez, J.E., Turner, P.J., McNeil, C., Sanford, T.B., 2015. Numerical modeling of circulation in high-energy estuaries: A Columbia River estuary benchmark. Ocean. Model. 88, 54–71.
Knudsen, M., 1900. Ein Hydrographische Lehrsatz. Ann. Hydrogr. Mar. Meteorol. 28, 316–320.
Lucas, L.V., Thompson, J.K., Brown, L.R., 2009. Why are diverse relationships observed between phytoplankton biomass and transport time? Limnol. Oceanogr. 54, 381–390.
Needoba, J.A., Peterson, T.D., Johnson, K.S., 2012. Molecular biological technologies for ocean sensing. Chapter method for the quantification of aquatic primary production and net ecosystem metabolism using. In: Situ Dissolved Oxygen Sensors. Humana Press, Totowa, NJ, pp. 73–101.
Peterson, T., Golda, R., Garcia, M., Li, B., Maier, M., Needoba, J., Zuber, P., 2013. Associations between Mesodinium rubrum and cryptophyte algae in the Columbia River estuary. Aquat. Microb. Ecol. 68, 117–130.
Prahl, F., Small, L., Eversmeyer, B., 1998. Biogeochemical characterization of suspended particulate matter in the Columbia River estuary. Oceanogr. Lit. Rev. 45, 1324.
Roegner, G.M., Needoba, J.A., Baptista, A., 2011. Coastal upwelling supplies oxygen-depleted water to the Columbia River Estuary. PLoS One 6, e18672.
Shen, J., Haas, L., 2004. Calculating age and residence time in the tidal York River using three-dimensional model experiments. Estuar. Coast. Shelf Sci. 61, 449–461.
Small, L.F., Prahl, F.G., 2004. A particle conveyor belt process in the Columbia River estuary: evidence from chlorophylla and particulate organic carbon. Estuaries 27, 999–1013.
Smith, M.W., Davis, R.E., Youngblut, N.D., Kärnä, T., Herfort, L., Whitaker, R.J., Metcalf, W.W., Tebo, B.M., Baptista, A.M., Simon, H.M., 2015. Metagenomic evidence for reciprocal particle exchange between the mainstem estuary and lateral bay sediments of the lower Columbia River. Front. Microbiol. 6.
Swaney, D., Smith, S., Wulff, F., 2011. The LOICZ Biogeochemical modeling protocol and its application to estuarine ecosystems. In: Wolanski, E., McLusky, D. (Eds.), Treatise on Estuarine and Coastal Science. Academic Press, Waltham, pp. 135–159.
Valle-Levinson, A., 2010. Contemporary Issues in Estuarine Physics. Cambridge Books Online. Cambridge University Press.
Warner, J., Rockwell Geyer, W., Arango, H., 2010. Using a composite grid approach in a complex coastal domain to estimate estuarine residence time. Comput. Geosci. 36, 921–935.
Wolanski, E., 2007. Estuarine Ecohydrology. Elsevier.
Zhang, W.G., Wilkin, J.L., Schofield, O.M.E., 2010. Simulation of water age and residence time in New York bight. J. Phys. Oceanogr. 40, 965–982.
Zhang, Y., Baptista, A.M., 2008. SELFE: a semi-implicit Eulerian-Lagrangian finite-element model for cross-scale ocean circulation. Ocean. Model. 21, 71–96.
Zimmerman, J.T.F., 1988. Estuarine residence times. In: Kierfve, B. (Ed.), Hydrodynamics od estuaries, vol. 1, pp. 75–84 (Chapter 6).